VIP Conductive Paper Very Important Paper

DOI: 10.1002/anie.201307830

Written-in Conductive Patterns on Robust Graphene Oxide Biopaper by Electrochemical Microstamping**

*Kesong Hu, Lorenzo S. Tolentino, Dhaval D. Kulkarni, Chunhong Ye, Satish Kumar, and Vladimir V. Tsukruk**

Although graphene-based flexible "paper" materials[1–4] made by vacuum-assisted assembly have been introduced as prospective superior carbon-only replacements of inorganic-based nanocomposites with excellent mechanical properties, their further progress as protective coatings, electronic substrates, electromagnetic shielding, and electromechanical elements is limited by several issues related to their integration in practical device environment.[5–13] Very limited options for inducing electrical conductivities and long-term stability under wet conditions are the most critical issues for further developments.[14–21] The epoxide, hydroxy, carbonyl, and carboxy groups of graphene oxide enable aqueous processibility and enhance interfacial interactions and cross-linking (Supporting Information, Figure S1). The variable content of water molecules, which is a common "binder" of graphene oxide paper through hydrogen bonding, affects the reliability of the mechanical performance of the graphene oxide paper.[1,13] Moreover, graphene oxide paper is susceptible to water plasticization and easily loses its mechanical integrity in humid and wet conditions and during chemical or thermal reduction process as to fabricate conductive flexible paper.

To tackle this challenge, many studies have focused on strengthening the graphene oxide papers by chemical cross-linking.[18] The heterogeneous nature of the surface of graphene oxide flakes with hydrophobic domains isolated by highly oxidized hydrophilic domains makes it difficult to apply traditional strategies for making strong layered nanocomposites with conventional organic binders and cross-linking strategies.[7,22,23] Moreover, unlike "bucky paper" or other nanocomposites made from carbon nanotubes,[24,25] the integration of these graphene oxide nanocomposite films into the flexible electronic devices calls for further reduction by chemical, electrochemical, thermal, photothermal, or hydrothermal routes, which usually involves harsh and toxic chemicals or intensive thermal treatments, thus consequently damaging the structural integrity of the graphene papers and reducing their stability.[26–29] These conventional reducing techniques also lack selectivity and patternability means, making it challenging to precisely control the reduced area and fabricate conductive circuitries.

Herein, we report on a novel way for facile writing-in of electrically conductive microscopic patterns by a spatially localized electrochemical reduction with micron-scale resolution on robust bio-graphene paper under ambient conditions. We found that the "microstamping" with preshaped aluminum foil in direct physical contact with the surface of graphene oxide biopaper can spontaneously and locally reduce selected regions of graphene oxide in ambient conditions resulting in excellent local electrical conductivity. Such a readily controlled and "green" treatment combined with the ability of both selective electrochemical reduction (surface regions and depth) creates electrically conductive paper materials without compromising the mechanical or environmental stability. The shape and depth of the reduced conductive regions are controllable by microstamping conditions. These robust biopapers with excellent wet stability that facilitates the writing-in technique were assembled by replacing synthetic binders with a heterogeneous hydrophilic–hydrophobic biopolymer "binder"—silk fibroin, which matches the random domain surface functionalities of graphene oxides.[30–32] Moreover, in contrast to other synthetic binders, silk fibroin is mechanically strong, optically transparent, biocompatible, biodegradable, and can serve as an additional reducing agent.[33,34]

Vacuum-assisted filtration was used to fabricate layered "paper" from the homogeneous mixture of graphene oxide and silk fibroin similar to literature methods but with special efforts to prevent fast coagulation of biopolymer solution (see Experimental Section and Supporting Information).[1,2,35] The resulting 2D stacking of the graphene oxide flakes within several-micron-thick freely standing paper is presented in Figure 1a. The root-mean-square surface roughness measured by atomic force microscopy (AFM) is 0.30 ± 0.06 μm per 100 μm^2 square area for the as prepared paper, indicating their uniformity (below 4% variation in thickness; Figure 1b). The incorporation of silk fibroin in the stacks of graphene oxide flakes is confirmed quantitatively by X-ray photoelectron spectroscopy (XPS), which shows the silk fibroin added in the mixture is effectively bonded to the graphene oxide flakes and retained in the final films (Table S1). The interlayer spacing of the initial graphene oxide paper as measured from (001) peak of the X-ray diffraction (XRD) data is 0.81 nm, which is close to the

[*] K. Hu, L. S. Tolentino, Dr. D. D. Kulkarni, Dr. C. Ye, Prof. S. Kumar, Prof. V. V. Tsukruk
School of Materials Science and Engineering
Georgia Institute of Technology
Atlanta, GA 30332-0245 (USA)
E-mail: vladimir@mse.gatech.edu
Homepage: http://polysurf.mse.gatech.edu

[**] We appreciate the technical support from Dr. Yaodong Liu and An-Ting Chien for the tensile measurements. We thank the financial support provided by the Air Force Office for Scientific Research Grant FA9550-11-1-0233 and Grant FA9550-09-1-0162 (BIONIC Center), and from the Semiconductor Research Corporation Grant 2008J1864.1281.

Supporting information for this article is available on the WWW under http://dx.doi.org/10.1002/anie.201307830.

 © 2013 Wiley-VCH Verlag GmbH & Co. KGaA, Weinheim

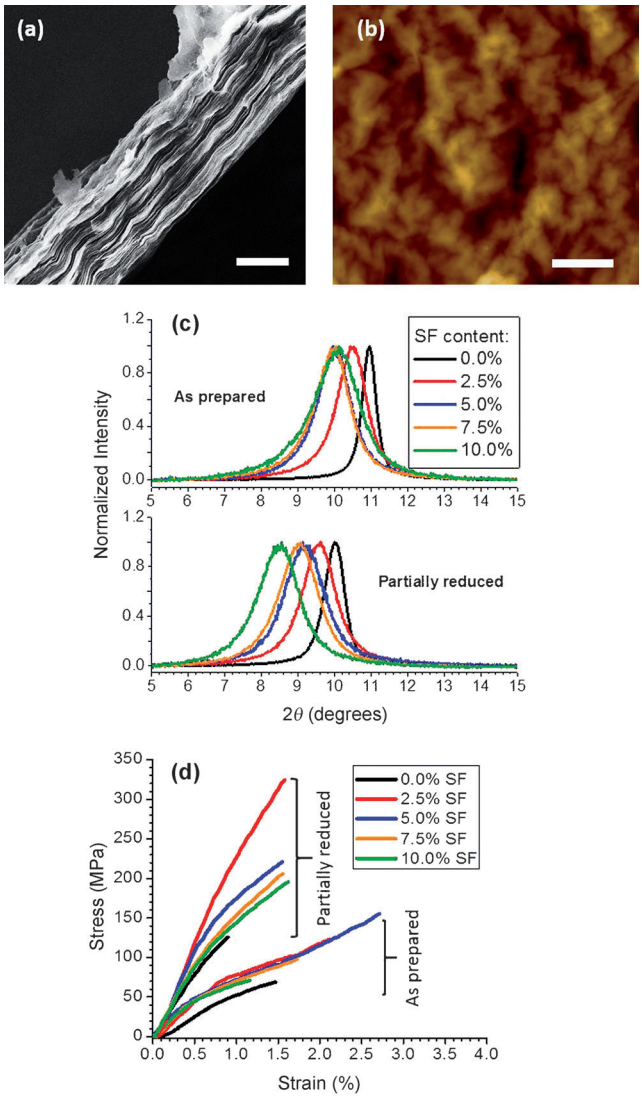

Figure 1. Morphologies of the graphene oxide silk fibroin films: a) SEM micrograph (scale bar: 5 μm) of the fractured cross section of the silk fibroin intercalated graphene oxide film. b) AFM surface topography before reduction (scale bar: 20 μm, *z*-range: 6 μm). c) XRD data for the graphene oxide nanocomposite films with various silk fibroin (SF) contents before (top) and after electrochemical reduction (bottom). d) Representative stress-strain curves of the graphene oxide biopaper before and after partial reduction.

common interlayer spacing for these materials.[36,37] Addition of a small quantity of silk fibroin (below 10%) results in the gradual increase of the interlayer spacing to 0.89 nm, which indicates the uniform intercalation of silk fibroin molecules (Figure 1c top, and Figure S2). The width of the peaks also progressively increases, indicating fewer stacking layers of the graphene oxide flakes from around 20 for pure graphene oxide paper to around 10 for higher silk content due to the excessive intercalation of silk fibroin and flakes mis-stacking defects (Table S1). Note that the overall content of silk binder within paper calculated from XPS and XRD data is close to the initial silk content in solution (except for the highest, 10%) which indicates effective intercalation of silk macromolecules for modest (below 7%) silk concentrations in initial solution.

The mechanical properties of as-prepared pure graphene oxide paper with the elastic modulus value of 7 GPa and ultimate strength of 60 MPa are on par with literature data (Figure 1d and Figure S3).[13] Adding silk binder results in dramatic improvement of mechanical performance: the ultimate stress, ultimate strain, elastic modulus, and toughness reach 153 MPa, 2.8%, 13 GPa, and 2.6 MJ m^{-3} at 5% silk fibroin, respectively, which are correspondingly two-three times higher than those of the pure graphene oxide paper. The increased stability in wet environment compared to traditional graphene oxide papers has been confirmed as well with no visible swelling or delamination occurring under a stream of water (Video S1).

Most importantly, the effective writing-in method for facile fabrication of electrically conductive patterns of any shape with high selectivity has been discovered for the biopapers by applying preshaped aluminum foil under wet ambient conditions. The resulting materials demonstrate the highly localized nature of the chemical reduction process (Figure 2). Such microcontact-controlled reduction to the

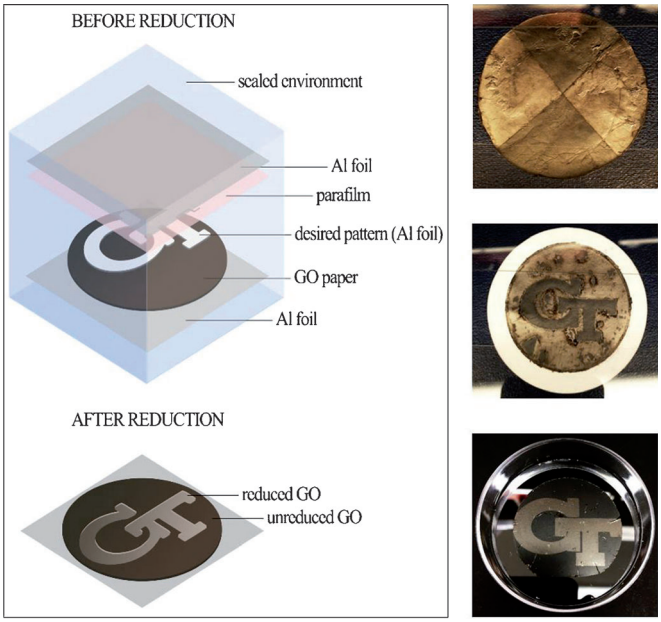

Figure 2. The reduction setup using electrochemical microstamping method. The resulting patterned graphene oxide biopaper specimens are shown on the right (from top to bottom): checker pattern (freely standing paper reduced by preshaped aluminum foils), GT logo with the background reduced (on filter paper reduced by preshaped aluminum foils, submerged in water), and GT logo reduced by an aluminum deposited pattern, transferred to a silicon wafer. The reduced areas have metallic luster and are light gray in color. The diameter of the all specimens is around 40 mm.

conductive state can be readily implemented with micro-scale lateral resolution below 10 μm for manually cut foil patterns and is potentially comparable to traditional photolithography or laser etching (Figure 2 and Figure 3).[38] Indeed, patterned metallic deposition techniques have been tested in our

 © 2013 Wiley-VCH Verlag GmbH & Co. KGaA, Weinheim

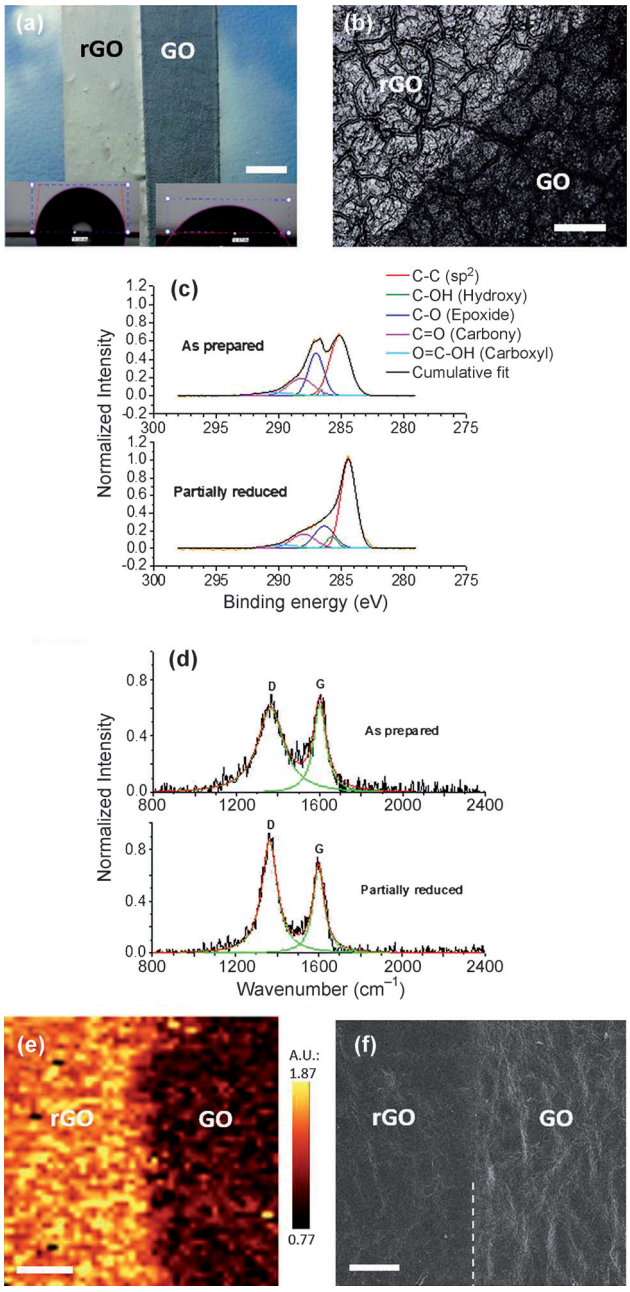

Figure 3. Microstamping of graphene oxide biopaper: a) Micrographs (scale bar: 5 mm) of two strips along with contact angle measurements before (right, GO) and after (left, rGO) reduction. b) Reflective optical micrograph (scale bar: 200 μm) showing the border of the partially reduced region. c) XPS C1 s high resolution spectra, and d) Raman spectra before (top) and after (bottom) selective reduction; e) Raman mapping (scale bar: 20 μm) of the I_D/I_G ratio and f) SEM image (scale bar: 300 μm) of the border between the reduced and the pristine regions.

preliminary study to demonstrate the possible high definition process, which will be further discussed in detail elsewhere (Figure 2, lower right).

The effective chemical reduction of graphene oxide by direct physical contact with aluminum foil is first reflected by the spectacular shift in color (dark brown to gray) and the appearance of metallic luster of the films (Figure 2, Figure 3 a,b). The change in color and enhanced luster of initial black paper suggests the narrowing down of the band gap of this material, which in turn indicates the reconstruction of the sp^2 hybridization chemical structures.[39] In addition, the contact angle of the film increased from 51° to 81°, showing a significant increase in hydrophobicity as expected for surfaces with increase graphitization. It is also of note that the surface roughness of the reduced regions is not changed compared to the as prepared samples, indicating absence of stresses and buckling at the interfacial regions between pristine and reduced regions (Figure S4).

Changes in chemical functionality of graphene oxide flakes are further confirmed by XPS, XRD, energy-dispersive X-ray (EDX) analysis, and Raman spectroscopy (Figure 3, Figure S5 and S6). Indeed, the C/O ratio increased from 2.2 to 3.5, indicating effective removal of the oxygen-containing functionalities (Figure S1b and Table S1).[39] The presence of 9 wt % Al^{3+} is also identified independently by XPS and EDX (Figure S5 and Table S1). The aluminum ions are distributed in interior space of the films as can be confirmed from the increase of the interlayer spacing by 0.11 ± 0.04 nm, which is consistent with intercalation of partial monolayer ions (Figure 1 c lower part and Figure S2).[14] The high-resolution XPS C1s scan shows that the relative intensity of the signals arising from the epoxide group decreased by 29 %, and that of the graphitic carbon increased by 19 % after the reduction, which is a clear sign of the effective removal of oxidized chemical groups and the restoration of the conducting sp^2 hybridized carbon (Figure 3 c).[21] Finally, Raman spectra show the width of the D band decreases and the I_D/I_G ratio increases from 0.96 to 1.27, which is another recognized sign of the homogenization of the sp^3 carbons through the removal of oxygen-caused defects, which also occurred in highly localized manner (Figure 3 d and e).[40] Raman mapping reveals narrow microscopic transitional zone between pristine and transformed surface regions similar to that observed in optical microscopies and scanning electron microscopy (SEM) of surfaces (Figure 3 b,e,f and Figure S6).

Considering these results, we can suggest that these changes of chemical functionality are due to the presence of aluminum, which is an active reducing metal with a standard reduction potential (E^0_{Al}) of −1.66 V.[29] Aluminum can reduce other materials with a standard reduction potential higher than E^0_{Al} including graphene oxide (e.g. $E^0_{GO} = 0 \pm 0.6$ V depending on oxidization state[29,41,42]) according to the following electrochemical path [Eq. (1),(2)]:[43]

$$Al \rightarrow Al^{3+} + 3e^-; \qquad E^0_{Al} = -1.66\ V \tag{1}$$

$$a\,GO + b\,H^+ + b\,e^- \rightarrow a\,rGO + b/2\,H_2O \qquad E^0_{GO} \approx 0 \pm 0.6\ V \tag{2}$$

It is important to note that although acidic conditions facilitate the faster reduction of graphene oxide, the chemical reaction can be conducted even in neutral condition at pH 7 ± 0.4 and room temperature.[43] Moreover, depth-distribution of the transformed interior volume obtained with SEM on fractured region confirms gradual progression of the reaction from the surface to the interior (Figure 4 a–c). Darker regions in proximity to the surface being in contact with aluminum

© 2013 Wiley-VCH Verlag GmbH & Co. KGaA, Weinheim

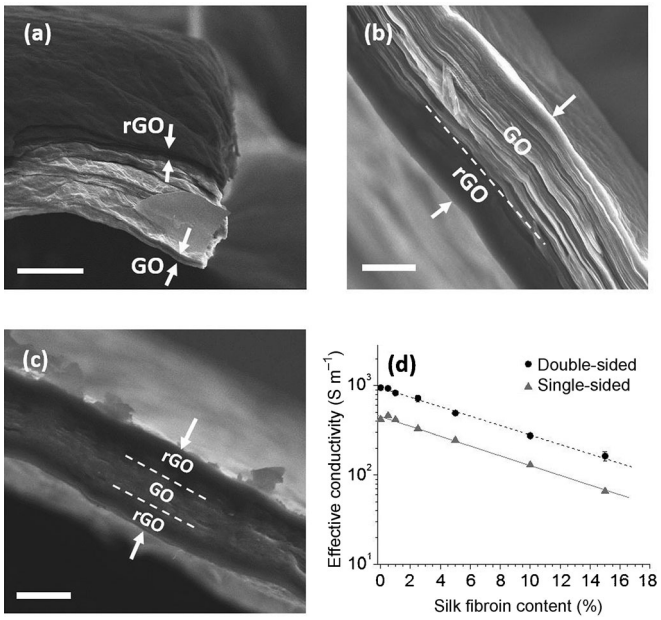

Figure 4. SEM micrographs of the partially reduced graphene oxide biopaper and their electrical conductivity. a) SEM micrograph (scale bar: 20 μm) of a fractured biopaper with the reduced top layer (dark) and the pristine non-reduced bottom layers (bright). The cross sections with the b) bottom surface reduced, and c) both surfaces reduced (scale bar: 5 μm). The white arrows indicate the thicknesses of the biopaper. d) The electrical conductivities of the uniformly reduced graphene oxide biopaper with various contents of silk fibroin. Data points for the single-sided samples corresponding to the scenario in (b), and those for the double-sided samples corresponding to the scenario in (c).

foil correspond to conductive, transformed sub-surface region while brighter regions indicate high surface charges on the pristine non-conductive graphene oxide material. Stopping the electrochemical reaction at a certain time resulted in conversion only to a certain depth that is controlled by the electronic connectivity of the graphene oxide to the aluminum metal as in the primary batteries (Figure 4b and c). Placing aluminum foils on both surfaces of the film allows concurrent propagation of the electrochemical transformation from both surfaces and results in interior transformation that occurs twice as fast (Figure S7).

As a result of this electrochemical reaction, the conductivity of the transformed graphene oxide regions reaches 1350 S m^{-1} for completely transformed paper with 2.5% of silk binder (Figure S7). This value is comparable to the values of 1700–2100 S m^{-1} of the graphene oxide papers uniformly reduced by traditional harsh methods.[29,44] The effective conductivity of the single-side treated film is exactly half of the double-side treated film, which suggests the critical role of the reduction depth propagation in material conductivity (Figure 4d). We suggest that adding insulating binder results in lower conductivity as a result of the interruption of the propagation path for electrons by the presence of the aggregated silk and defects in flake stacking (Figure 4d).

It is critically important that after chemical transformation by electrochemical reduction, the paper shows improved mechanical properties, in striking contrast to the traditional reduction techniques that inevitably damage the binder components (Figure S3). The ultimate strength of the transformed films reaches a very high value of 300 MPa at low silk content, which results also in the highest toughness of 2.8 MJ m^{-3} among all the samples tested in this study (Figure 1d). Moreover, the elastic modulus of the reduced graphene paper increased almost three-fold to 26 GPa as a result of defect reduction and the Al ion doping.[14] The increase in the mechanical strength may be also caused by additional cross-linking and the reducing ability of silk backbones.[45] The mechanical properties of the graphene biopapers observed herein are among the best of the traditional graphene-based papers reported to date.[7,14,19,21] For example, drop-cast graphene oxide silk fibroin films have comparable ultimate strain at 1.8% but much lower tensile strength and elastic modulus.[19] A graphene oxide polyvinyl alcohol (PVA) film that has been reduced by hydroiodic acid (HI) has a much lower strength and modulus.[12] Chemically cross-linked graphene oxide (polydopamine)polyethyleneimine (PEI) films exhibit high elastic modulus up to 103 GPa but lower tensile strength of 210 MPa and only 0.2% strain-to-failure, which is a common problem for brittle cross-linked graphene paper.[18]

In summary, we demonstrated that electrically conductive patterns with a micron resolution can be efficiently written-in by electrochemical microstamping on robust and wet-stable graphene oxide biopapers under neutral aqueous conditions and at room temperature. The outstanding mechanical and electrical conductive properties of the graphene biopaper makes it an excellent candidate for structural and functional components, holding promising potentials in the emerging applications of chemical barriers, electromagnetic interference shielding, sensory skin, and potentially biodegradable, flexible papers with written-in electrical circuitry for bioelectronics devices.

Experimental Section

Materials and sample fabrication: Silk fibroin was extracted and purified from cocoons of *Bombyx mori* silkworms as described elsewhere.[20,33,46] Graphene oxide suspension (0.15 wt%) was prepared using Hummers method.[47] The pH value of the graphene oxide suspension was adjusted to 12 using 0.25 M sodium hydroxide immediately before mixing with silk fibroin solution at various ratios. Then the mixed suspension was filtered using a vacuum filtration system (Figure S8). The films were reprotonated and neutralized in Nanopure water (18.2 MΩ cm, Barnstead). The dried films were dampened by Nanopure water immediately before being sandwiched between two pieces of thin aluminum foil (no coating as confirmed by EDX and XPS) to induce chemical reduction. (See details in Supporting Information.)

Characterizations: Stress-strain curves of the films were collected by tensile testing the $2 \pm 0.2 \times 30$ mm strips with a gap between grips of 10 mm at room temperature (RSA III Dynamic Mechanical Analyzer, TA Instruments). SEM micrographs were captured by Hitachi 3400 SEM. AFM was done using ICON AFM (Bruker) in soft tapping mode.[48] XRD data were measured by X'Pert Pro Alpha-1 diffractometer. XPS spectra were collected by Thermal Scientific K-alpha XPS instrument; Raman spectra and maps were captured by a WiTek Alpha 300R confocal Raman microscope.[49] Electrical conductivity was measured by 4-probe method.

 © 2013 Wiley-VCH Verlag GmbH & Co. KGaA, Weinheim

Received: September 5, 2013
Published online: November 8, 2013

Keywords: conductive paper · electrical conductivity · graphene · mechanical properties · silk

[1] D. A. Dikin, S. Stankovich, E. J. Zimney, R. D. Piner, G. H. B. Dommett, G. Evmenenko, S. T. Nguyen, R. S. Ruoff, *Nature* **2007**, *448*, 457.
[2] Z. An, O. C. Compton, K. W. Putz, L. C. Brinson, S. T. Nguyen, *Adv. Mater.* **2011**, *23*, 3842.
[3] K. W. Putz, O. C. Compton, M. J. Palmeri, S. T. Nguyen, L. C. Brinson, *Adv. Funct. Mater.* **2010**, *20*, 3322.
[4] O. C. Compton, S. W. Cranford, K. W. Putz, Z. An, L. C. Brinson, M. J. Buehler, S. T. Nguyen, *ACS Nano* **2011**, *6*, 2008.
[5] E. Munch, M. E. Launey, D. H. Alsem, E. Saiz, A. P. Tomsia, R. O. Ritchie, *Science* **2008**, *322*, 1516.
[6] M. Yang, Y. Hou, N. A. Kotov, *Nano Today* **2012**, *7*, 430.
[7] D. D. Kulkarni, I. Choi, S. S. Singamaneni, V. V. Tsukruk, *ACS Nano* **2010**, *4*, 4667.
[8] C. Jiang, S. Markutsya, V. V. Tsukruk, *Adv. Mater.* **2004**, *16*, 157.
[9] C. Jiang, S. Markutsya, Y. Pikus, V. V. Tsukruk, *Nat. Mater.* **2004**, *3*, 721.
[10] Z. Xu, H. Sun, X. Zhao, C. Gao, *Adv. Mater.* **2012**, *24*, 188.
[11] P. Podsiadlo, A. K. Kaushik, E. M. Arruda, A. M. Waas, B. S. Shim, J. Xu, H. Nandivada, B. G. Pumplin, J. Lahann, A. Ramamoorthy, N. A. Kotov, *Science* **2007**, *318*, 80.
[12] Y.-Q. Li, T. Yu, T.-Y. Yang, L.-X. Zheng, K. Liao, *Adv. Mater.* **2012**, *24*, 3426.
[13] Y. Gao, L.-Q. Liu, S.-Z. Zu, K. Peng, D. Zhou, B.-H. Han, Z. Zhang, *ACS Nano* **2011**, *5*, 2134.
[14] S. Park, K.-S. Lee, G. Bozoklu, W. Cai, S. T. Nguyen, R. S. Ruoff, *ACS Nano* **2008**, *2*, 572.
[15] H. Kim, A. A. Abdala, C. W. Macosko, *Macromolecules* **2010**, *43*, 6515.
[16] H. Chen, M. B. Müller, K. J. Gilmore, G. G. Wallace, D. Li, *Adv. Mater.* **2008**, *20*, 3557.
[17] R. J. Young, I. A. Kinloch, L. Gong, K. S. Novoselov, *Compos. Sci. Technol.* **2012**, *72*, 1459.
[18] Y. Tian, Y. Cao, Y. Wang, W. Yang, J. Feng, *Adv. Mater.* **2013**, *25*, 2980.
[19] L. Huang, C. Li, W. Yuan, G. Shi, *Nanoscale* **2013**, *5*, 3780.
[20] K. Hu, M. K. Gupta, D. D. Kulkarni, V. V. Tsukruk, *Adv. Mater.* **2013**, *25*, 2301.
[21] Q. Cheng, M. Wu, M. Li, L. Jiang, Z. Tang, *Angew. Chem.* **2013**, *125*, 3838; *Angew. Chem. Int. Ed.* **2013**, *52*, 3750.
[22] J. Kim, L. J. Cote, F. Kim, W. Yuan, K. R. Shull, J. Huang, *J. Am. Chem. Soc.* **2010**, *132*, 8180.
[23] I. Choi, D. D. Kulkarni, W. Xu, C. Tsitsilianis, V. V. Tsukruk, *Langmuir* **2013**, *29*, 9761.
[24] X. Zhang, T. V. Sreekumar, T. Liu, S. Kumar, *J. Phys. Chem. B* **2004**, *108*, 16435.
[25] H. Guo, T. V. Sreekumar, T. Liu, M. Minus, S. Kumar, *Polymer* **2005**, *46*, 3001.
[26] J. Yuan, L.-P. Ma, S. Pei, J. Du, Y. Su, W. Ren, H.-M. Cheng, *ACS Nano* **2013**, *7*, 4233.
[27] T. Kuila, A. K. Mishra, P. Khanra, N. H. Kim, J. H. Lee, *Nanoscale* **2013**, *5*, 52.
[28] M. F. El-Kady, V. Strong, S. Dubin, R. B. Kaner, *Science* **2012**, *335*, 1326.
[29] Z. Fan, K. Wang, T. Wei, J. Yan, L. Song, B. Shao, *Carbon* **2010**, *48*, 1686.
[30] D. Porter, F. Vollrath, *Adv. Mater.* **2009**, *21*, 487.
[31] E. Kharlampieva, D. Zimnitsky, M. Gupta, K. N. Bergman, D. L. Kaplan, R. R. Naik, V. V. Tsukruk, *Chem. Mater.* **2009**, *21*, 2696.
[32] H. Shulha, C. W. Po Foo, D. L. Kaplan, V. V. Tsukruk, *Polymer* **2006**, *47*, 5821.
[33] C. Jiang, X. Wang, R. Gunawidjaja, Y. H. Lin, M. K. Gupta, D. L. Kaplan, R. R. Naik, V. V. Tsukruk, *Adv. Funct. Mater.* **2007**, *17*, 2229.
[34] G. H. Altman, F. Diaz, C. Jakuba, T. Calabro, R. L. Horan, J. Chen, H. Lu, J. Richmond, D. L. Kaplan, *Biomaterials* **2003**, *24*, 401.
[35] D. Li, M. B. Muller, S. Gilje, R. B. Kaner, G. G. Wallace, *Nat. Nanotechnol.* **2008**, *3*, 101.
[36] R. Jalili, S. H. Aboutalebi, D. Esrafilzadeh, K. Konstantinov, S. E. Moulton, J. M. Razal, G. G. Wallace, *ACS Nano* **2013**, *7*, 3981.
[37] S. Park, R. S. Ruoff, *Nat. Nanotechnol.* **2009**, *4*, 217.
[38] E. Menard, M. A. Meitl, Y. Sun, J.-U. Park, D. J.-L. Shir, Y.-S. Nam, S. Jeon, J. A. Rogers, *Chem. Rev.* **2007**, *107*, 1117.
[39] S. Pei, H.-M. Cheng, *Carbon* **2012**, *50*, 3210.
[40] I. K. Moon, J. Lee, R. S. Ruoff, H. Lee, *Nat. Commun.* **2010**, *1*, 73.
[41] X. Mei, H. Zheng, J. Ouyang, *J. Mater. Chem.* **2012**, *22*, 9109.
[42] X. Cao, D. Qi, S. Yin, J. Bu, F. Li, C. F. Goh, S. Zhang, X. Chen, *Adv. Mater.* **2013**, *25*, 2957.
[43] J. O. M. Bockris, A. K. N. Reddy, *Modern Electrochemistry*, Plenum, New York, **1998**.
[44] S. Park, J. An, I. Jung, R. D. Piner, S. J. An, X. Li, A. Velamakanni, R. S. Ruoff, *Nano Lett.* **2009**, *9*, 1593.
[45] E. Kharlampieva, V. Kozlovskaya, B. Wallet, V. V. Shevchenko, R. R. Naik, R. Vaia, D. L. Kaplan, V. V. Tsukruk, *ACS Nano* **2010**, *4*, 7053.
[46] M. K. Gupta, S. Singamaneni, M. McConney, L. F. Drummy, R. R. Naik, V. V. Tsukruk, *Adv. Mater.* **2010**, *22*, 115.
[47] W. S. Hummers, R. E. Offeman, *J. Am. Chem. Soc.* **1958**, *80*, 1339.
[48] M. E. McConney, S. Singamaneni, V. V. Tsukruk, *Polym. Rev.* **2010**, *50*, 235.
[49] S. Singamaneni, M. Gupta, R. Yang, M. M. Tomczak, R. R. Naik, Z. L. Wang, V. V. Tsukruk, *ACS Nano* **2009**, *3*, 2593.

 © 2013 Wiley-VCH Verlag GmbH & Co. KGaA, Weinheim